

PAPER • OPEN ACCESS

## Rotational electrical impedance tomography using electrodes with limited surface coverage provides window for multimodal sensing

To cite this article: Mari Lehti-Polojärvi *et al* 2018 *Meas. Sci. Technol.* **29** 025401

View the [article online](#) for updates and enhancements.

# Rotational electrical impedance tomography using electrodes with limited surface coverage provides window for multimodal sensing

Mari Lehti-Polojärvi<sup>1,4</sup> , Olli Koskela<sup>1,4</sup> , Aku Seppänen<sup>2</sup> ,  
Edite Figueiras<sup>3</sup>  and Jari Hyttinen<sup>1</sup> 

<sup>1</sup> BioMediTech Institute and Faculty of Biomedical Sciences and Engineering, Tampere University of Technology, Tampere, Finland

<sup>2</sup> Department of Applied Physics, University of Eastern Finland, Kuopio, Finland

<sup>3</sup> International Iberian Nanotechnology Laboratory, Braga, Portugal

E-mail: [mari.lehti@tut.fi](mailto:mari.lehti@tut.fi) and [oli.koskela@tut.fi](mailto:oli.koskela@tut.fi)

Received 11 October 2017

Accepted for publication 3 November 2017


Published 17 January 2018



## Abstract

Electrical impedance tomography (EIT) is an imaging method that could become a valuable tool in multimodal applications. One challenge in simultaneous multimodal imaging is that typically the EIT electrodes cover a large portion of the object surface. This paper investigates the feasibility of rotational EIT (rEIT) in applications where electrodes cover only a limited angle of the surface of the object. In the studied rEIT, the object is rotated a full 360° during a set of measurements to increase the information content of the data. We call this approach limited angle full revolution rEIT (LAFR-rEIT). We test LAFR-rEIT setups in two-dimensional geometries with computational and experimental data. We use up to 256 rotational measurement positions, which requires a new way to solve the forward and inverse problem of rEIT. For this, we provide a modification, available for EIDORS, in the supplementary material. The computational results demonstrate that LAFR-rEIT with eight electrodes produce the same image quality as conventional 16-electrode rEIT, when data from an adequate number of rotational measurement positions are used. Both computational and experimental results indicate that the novel LAFR-rEIT provides good EIT with setups with limited surface coverage and a small number of electrodes.

Keywords: electrical impedance tomography, limited angle surface detection, rotational finite element method, multimodal imaging

 Supplementary material for this article is available [online](#)

(Some figures may appear in colour only in the online journal)



Original content from this work may be used under the terms of the [Creative Commons Attribution 3.0 licence](#). Any further distribution of this work must maintain attribution to the author(s) and the title of the work, journal citation and DOI.

<sup>4</sup> Authors contributed equally to this work.

## 1. Introduction

Electrical impedance tomography (EIT) is a high-speed, non-destructive and non-invasive imaging technique that has applications in several fields that include medical imaging, industrial process tomography and geophysical surveying. Traditionally in EIT, current stimulations and voltage measurements are carried out using equally spaced electrodes on the surface of the object (i.e. sample with inclusions of interest) [1, 2]. Based on these measurements, an image is reconstructed that represents the conductivity distribution of the object. The major advantages of EIT are high temporal resolution and that no ionizing radiation is applied as, for example, in x-ray computed tomography. The main drawback of EIT is its relatively poor spatial resolution. One approach to enhance spatial resolution is to use rotational EIT (rEIT), a method that increases the number of independent measurements [3–7].

EIT is a functional imaging method that could become a valuable tool in multimodal applications [8–11]. The combination of EIT and a structural imaging method, such as ultrasonic imaging, could provide robust diagnostic or research tools. One challenge in simultaneous multimodal imaging is that in typical settings the EIT electrodes cover a large portion of the object surface, and therefore the area left for other sensors is very limited.

To attain new applications for multimodal EIT with good spatial resolution, we propose a rEIT setup where stationary electrodes span a limited angle near to the object surface and measurements are acquired along  $360^\circ$  (asymmetric electrode configurations) or  $180^\circ$  (symmetric electrode configurations) rotation of the object. We call this approach limited angle full revolution rotational EIT (LAFR-rEIT).

Figure 1 illustrates one scheme of a LAFR-rEIT setup, where electrodes cover less than half of the object surface and additional measurements are possible at the sides that are free from EIT electrodes. This particular configuration will allow multimodal measurements as, for example, the combination of other tomographic methods with rEIT.

Previously presented rEIT setups have applied electrode arrays that are evenly distributed around the circumference of the object. Rotating this kind of electrode array only increases the acquired independent data within rotation angles smaller than the distance between the centres of the neighbouring electrodes. For example, in a conventional 16-electrode setup, rEIT measurements are obtained within  $22.5^\circ$  rotation. LAFR-rEIT, on the other hand, is expected to benefit from measurements within full  $360^\circ$  or  $180^\circ$  rotation. In addition, LAFR-rEIT enables relatively simple instrumentation due to the small number of electrodes.

LAFR-rEIT could be used to image objects that can be rotated while the electrodes remain at rest, or vice versa. We present a case where the object is rotated in conductive aqueous solution, as is shown in figure 1. Such setups are relevant in applications where EIT is used for imaging specimens of materials and/or structures, e.g. for non-destructive testing of concrete [12] and biological samples [13].

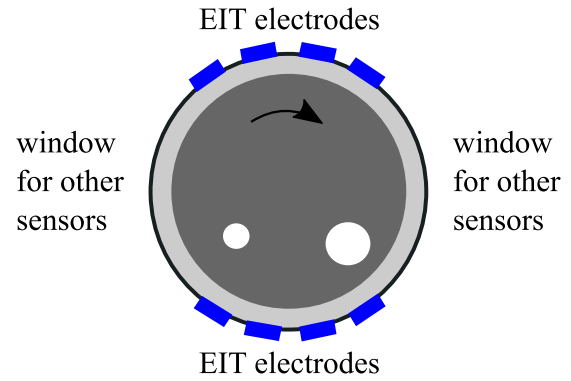


**Figure 1.** Schematic of the rotational measurement setup comprising a rotating object (dark grey) with inclusions (white circles), aqueous solution (light grey) and electrodes used for EIT. Additional modality can be measuring either backscattering or transmission and has possible contact sites on the left and right sides of the object.

The purpose of this paper is to introduce LAFR-rEIT approach and to study whether it could provide image quality comparable with 16-electrode rEIT. The efficacy of LAFR-rEIT is evaluated in both computational models (sections 2.3 and 3) and experimental measurements on two-dimensional (2D) phantoms (sections 2.4 and 4). We anticipate this work will open new possibilities for high-quality multimodal imaging of material specimens.

## 2. Methods

### 2.1. Image reconstruction

This section presents the mathematical model for a rEIT setup. Using the model, the number and placement of the electrodes and the number of rotational measurement positions can be chosen arbitrarily.

Let  $\sigma \in \Omega$  mark the conductivity distribution inside a given object  $\Omega$ . For each measurement position  $k$  and rotated object  $\Omega_k$ , we have a conductivity distribution  $\sigma_k \in \Omega_k$  in the rotated coordinates. The model used for measurement  $V_k$  using the complete electrode model is given in [14] and is of the form:

$$V_k = U(\sigma_k) + n_k, \quad (1)$$

where  $U$  is the forward model and  $n_k$  is a noise term.

We modelled the rotation of the coordinates in  $k$ th position using a linear mapping  $M_k$  so that for conductivity distribution  $\sigma \in \Omega$  in initial position, the rotated coordinates are given by  $\Omega_k = M_k \Omega$  and  $\sigma_k = M_k \sigma$ . We assume that  $\sigma$  does not change during the rotation. For a finite element approximation  $\Omega = (e_i)$ , mapping  $M_k = (w_{i,j})_k$  is a weight matrix. Each weight  $w_{i,j}$  is the area of intersection of  $e_j$  and  $e_i$ , where  $e_i$  is rotated for the measurement angle  $\alpha_k$ . Rotation is illustrated in figure 2.

For a set of  $m$  measurements  $V_k$  ( $k \in [1, m] \subset \mathbf{N}$ ) with rotational measurement positions within  $\alpha_k \in [0, 2\pi]$ , the forward EIT model was written in stacked form as follows:

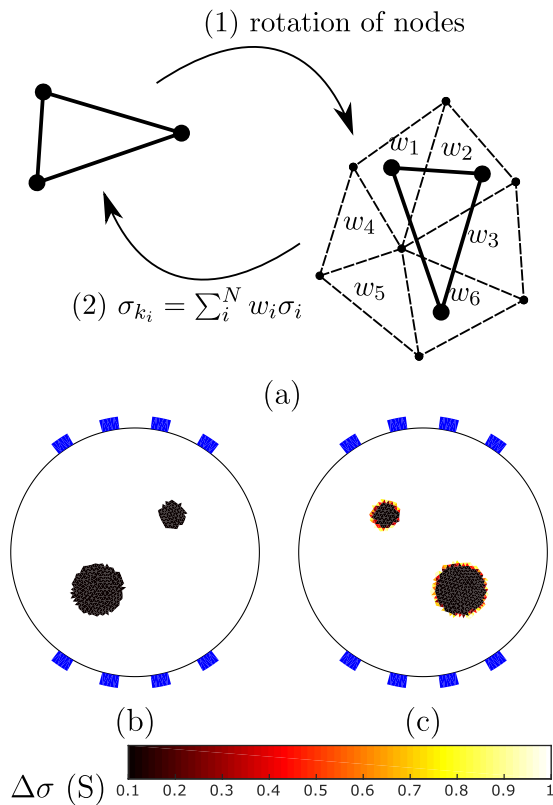


**Figure 2.** (a) For each element and each rotational position, weights of the mapping  $M$  are computed by (1) first rotating element coordinates around the centre of the mesh in the opposite direction and then calculating the areas of intersection  $w_i$  with underlying elements. (2) The element data value  $\sigma_k$  of the rotational position is assigned using these weights. (b) Phantom and (c) its rotation for 90 degrees.

$$\begin{bmatrix} V_1 \\ V_2 \\ \vdots \\ V_m \end{bmatrix} = \begin{bmatrix} U(M_1\sigma) \\ U(M_2\sigma) \\ \vdots \\ U(M_m\sigma) \end{bmatrix} + \begin{bmatrix} n_1 \\ n_2 \\ \vdots \\ n_m \end{bmatrix} \quad (2)$$

or

$$V_r = U_r(\sigma) + n_r. \quad (3)$$

We adapted the rEIT to the framework of linearised difference imaging. In difference imaging, EIT measurements (here, corresponding to  $m$  rotational measurement positions) of a temporally varying object are performed before and after the change in two stages. It should be noted that here this change is expected to be slow. Therefore the above assumption/approximation of the conductivity being non-varying during each set of rEIT measurements is valid. The conductivity distribution of the object is denoted before and after the change by  $\sigma^{(1)}$  and  $\sigma^{(2)}$ , respectively, and the corresponding EIT measurements by  $V_r^{(1)}$  and  $V_r^{(2)}$ .

To reconstruct the *change* of the conductivity  $\Delta\sigma = \sigma^{(2)} - \sigma^{(1)}$  on the basis of difference data  $\Delta V_r = V_r^{(2)} - V_r^{(1)}$ , the mapping  $U_r(\sigma)$  was linearized by writing the first order Taylor approximation:

$$U_r(\sigma) \approx U_r(\sigma_0) + J_r(\sigma - \sigma_0). \quad (4)$$

Here,  $\sigma_0$  is a linearization point and  $J_r$  denotes the Jacobian matrix of  $U_r(\sigma)$  at  $\sigma_0$ .

$$J_r = \begin{bmatrix} JM_1 \\ \vdots \\ JM_m \end{bmatrix}, \quad (5)$$

where  $J_r$  and  $J$ , respectively, denote the Jacobian matrices of  $U_r(\sigma)$  and  $U(\sigma)$  at  $\sigma_0$ .

Using the approximation (4) for both measurement sets  $V_r^{(1)}$  and  $V_r^{(2)}$ , the observation model (3) can be expressed in terms of differences as in the following:

$$\Delta V_r = J_r \Delta\sigma + \Delta n_r, \quad (6)$$

where  $\Delta n_r = n_r^{(2)} - n_r^{(1)}$  is the difference between the noise realisations  $n_r^{(1)}$  and  $n_r^{(2)}$ .

Due to the ill-posedness of the EIT inverse problem, the reconstruction of  $\Delta\sigma$  requires regularisation. Here, we used the Tikhonov regularised solution:

$$\widehat{\Delta\sigma} = \arg \min_{\Delta\sigma} \{ \|\Delta V_r - J_r \Delta\sigma\|^2 + \alpha \|L \Delta\sigma\|^2 \} \quad (7)$$

$$= (J_r^T J_r + \alpha L^T L)^{-1} J_r^T \Delta V_r, \quad (8)$$

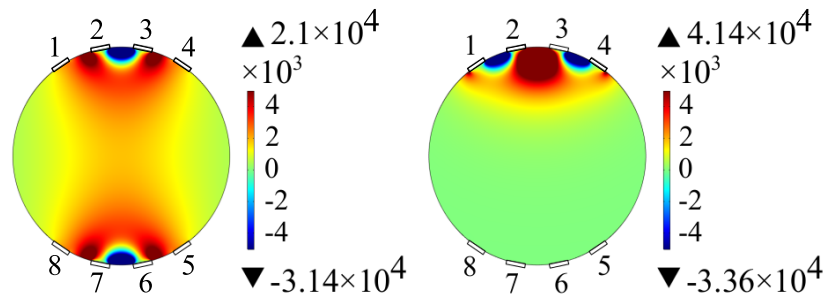
where  $L$  is a smoothness promoting regularisation matrix defined as a discrete second order differential operator, and  $\alpha$  is a regularisation parameter [15].

## 2.2. Stimulation and measurement patterns

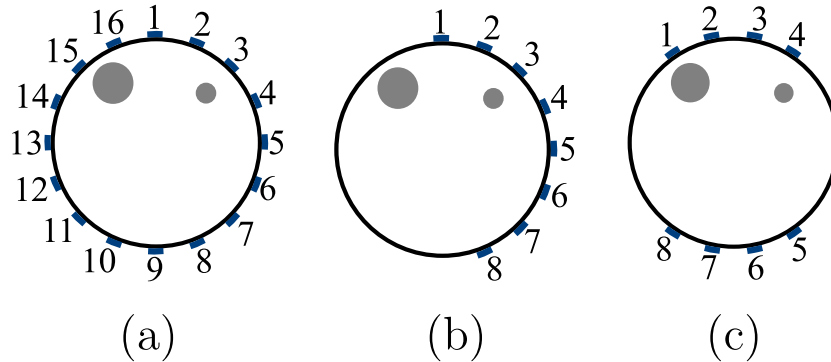
In EIT, it is preferable to have measurements both through the object (opposite electrodes) and near the surface of the object (adjacent electrodes). Based on the lead field theory [16], the sensitivity of a tetrapolar measurement can be calculated as a dot product of two current density vector fields. These fields are formed by feeding current to the current feeding electrodes, and reciprocally to the voltage measurement electrodes. This theory has been applied to design novel impedance measurement patterns for whole body EIT, tissue engineered systems and single cell measurements [17–20].

Figure 3 illustrates the sensitivity fields calculated for two different tetrapolar measurements in a LAFR-rEIT setup. These finite element simulations were carried out in Comsol Multiphysics v5.2a. The object was assumed to be homogeneous with conductivity of  $0.22 \text{ S m}^{-1}$  and relative permittivity of 80. A current of 3 mA was consecutively applied between electrode pairs. The pattern using opposing electrodes had high sensitivity close to the electrodes and in the centre of the object. The pattern using four adjacent electrodes had high sensitivity close to the electrodes, but low sensitivity elsewhere.

To maximise the information obtained by the limited number of electrodes in LAFR-rEIT, we chose to use all the available tetrapolar combinations for each electrode configuration. In this way, we were able to obtain patterns that were



**Figure 3.** Sensitivity field distributions ( $1/m^{-4}$ ) of two different measurement patterns. Current is injected between electrodes 2 and 7 (left) or 1 and 4 (right). Voltage is measured with electrodes 3 and 6 (left) or 2 and 3 (right).



**Figure 4.** (a) The standard 16-electrode configuration and ((b), (c)) two possible LAFR-rEIT configurations along with the phantom used in the numerical analysis. (b) Configuration HALF8 includes electrodes 1 to 8 and (c) OPP4 electrodes 1–4 and 9–12. Low conductivity inclusions are shown in grey.

both sensitive in the centre of the object and also sensitive at the edges. The rotation of the object allowed it to be measured from different angles, and thus the whole object was covered.

### 2.3. Numerical analysis

A numerical comparison of LAFR-rEIT using electrodes with limited angular coverage but full rotation, and a rotational 16-electrode model with full angular coverage electrodes but limited rotation was carried out. Full rotation is considered here to be  $180^\circ$  for LAFR-rEIT electrode configurations that are symmetrical to rotation after  $180^\circ$  and  $360^\circ$  for non-symmetrical electrode configurations. The 16-electrode model followed previous publications, for example [4], and shown in figure 4(a).

LAFR-rEIT electrode configurations followed two different approaches: the electrodes were placed either in two sets on opposite halves of the object, or in one set covering about half of the object surface. Both approaches allow measurements that are sensitive close to surface and through the object. Figures 4(b) and (c) shows the configurations with eight electrodes called HALF8 and OPP4, respectively. The angular difference between the centres of the stationary electrodes was  $22.5^\circ$  in all cases, and hence eight electrodes were distributed in the range of  $[0^\circ, 157.5^\circ]$  (HALF8), or  $[-33.75^\circ, 33.75^\circ] \cup [146.25^\circ, 213.85^\circ]$  (OPP4).

LAFR-rEIT was additionally tested with four and six electrode configurations called OPP2, OPP3, OPP4 + 2, HALF4 and HALF6, shown in figure 8. In HALF4, four electrodes

were positioned in an angular span of  $[0^\circ, 135^\circ]$  and in HALF6 six electrodes were positioned in a span of  $[0^\circ, 150^\circ]$

The phantom used in the simulations was circular with radius of 1 units and had 0.14 units size electrodes in all configurations. The electrode size equalled 18% object surface coverage with 16 electrodes. All inclusions in the phantoms had conductivity of 0.1 S while the background and aqueous solution had conductivity of 1 S. The inclusion diameters were 0.4 units and 0.2 units. The phantom is shown in figure 4. Input current in simulations is 1 ‘Amps’ (EIDORS unit in 2D).

For the 16-electrode model, data were simulated by rotating the object in an angular range of  $[0^\circ, 22.5^\circ - \frac{22.5^\circ}{N+1}]$ , where  $N$  is the number of rotational measurement positions. Outside this range the measurements become repeated due to symmetry. We studied the conventional single measurement position without rotation, and then rotational cases with 2, 3 and 6 measurement positions equally distributed within the mentioned range.

With the electrode configuration OPP4, data was simulated up to 256 measurement positions within  $180^\circ$  rotation. The other symmetric configurations, OPP2 and OPP3, were simulated with 32 rotational measurement positions in the same range. For asymmetric electrode configurations HALF4, HALF6, HALF8 and OPP4 + 2, data was simulated with 64 measurement positions in  $360^\circ$  rotation.

In all of the simulated data points  $V \in \mathbf{R}^n$ , the additive noise of two components was included yielding noisy data  $V_{\text{noisy}} \in \mathbf{R}^n$ :

$$V_{\text{noisy}} = V + p_1 \max(|V|) \cdot 10^{-4} + |V| p_2^T \cdot 10^{-3}.$$



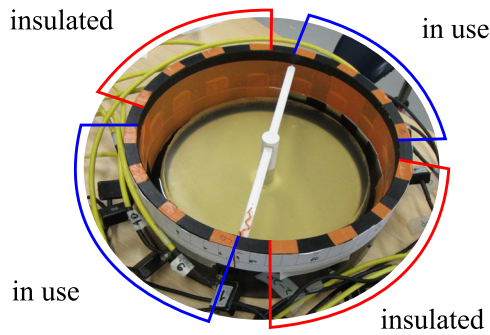


**Figure 5.** Measurement tank where eight of the 16 electrodes were insulated and eight electrodes were in use. A transparent cylindrical shaped gelatine phantom was placed on top of a rotation platform (white). A thin aqueous layer was between the object and the electrodes.

The first component is proportional to the maximum measured amplitude and the second component is proportional to each measurement. The vectors  $p_1, p_2 \in [-1, 1]^n$  were random numbers with uniform distribution.

#### 2.4. Experimental analysis

An experimental setup was used to test the feasibility of the LAFR-rEIT approach. The setup included a rotated object and OPP4 electrode configuration that was also numerically simulated as described above. An overview of the experimental setup is shown in figure 5. We used cylindrical shaped phantoms made of gelatine as a scaffold into which resistive inclusions were inserted. The phantoms were placed on a 3D printed platform (Polylactic acid) that was manually rotated. The phantoms and the platform were surrounded by an aqueous solution to preserve the structure of the object during its rotation and to ensure good electrical contact.

The gelatine scaffold for the phantoms was prepared from uncoloured 9.1% w/w Gelatine Powder (Dr.Oetker), 90.8% w/w tap water and 0.1% w/w sodium chloride (Maldon Sea Salt Flakes, Maldon Crystal Salt Co.). First, the gelatine powder was hydrated in cold tap water for 10 min. The mixture was then heated up to 74 °C and sodium chloride was added. The solution was then poured into a silicon mould (25 cm in diameter) and cooled in a refrigerator for 7 h for gelation. Prior to the measurements, the gelatine was stabilised at room temperature for about 9 h.

The tank was first filled with an aqueous solution (0.1% w/w sodium chloride and tap water) with a conductivity of 2.2 mS cm<sup>-1</sup>. The gelatine, with a conductivity of 2.4 mS cm<sup>-1</sup>, was placed on the rotation platform. The gelatine and platform were positioned in the middle of the tank (28 cm in diameter) and the height of the aqueous solution was adjusted to a height of 1 mm above the electrodes. After 30 min of stabilising the gelatine in the aqueous solution, the measurements were started.

Eight thin rectangular electrodes (25 mm × 45 mm) were attached to the inner surface of the tank. The measurements were conducted with the well-established KIT4 device presented in [21]. A sinusoidal 10 kHz 3.2 mA electrical current was used.

Three experimental phantoms were studied. In the first experimental case, we inserted a 50 mm diameter plastic tube into the gelatine. In the second case, we added a 29 mm diameter tube next to the tube in the case (1). In the third case, we replaced gelatine with one of the same composition and inserted two inclusions (50 mm and 29 mm in diameter) into opposite sides of it. The three cases are shown in photographs in figure 10. Prior to adding any tubes, both gelatine scaffolds (as in figure 5) were measured to obtain reference data for difference reconstruction.

The outer part of the measurement tank was marked with 32 equal length sectors over 180°. The sectors were used in combination with the stick in the rotation platform to allow correct rotation angles during the measurements. The data for all cases were acquired every 5.625° throughout the 180° rotation, leading to a total of 32 rotational measurement positions. The data were used to reconstruct the images with 1, 4, 16 and 32 positions by choosing only the first, every eighth, every second or all rotational measurement positions, respectively. In the reconstructions, we assumed the electrodes to be so thin that they can be modelled to be on the circumference of the region.

#### 2.5. EIDORS implementation of forward and inverse solver

We implemented the required modifications into EIDORS [22] functions to solve the forward and inverse problem of the rotational setting. These functions are provided in the supplementary material ([stacks.iop.org/MST/29/025401/mmedia](https://stacks.iop.org/MST/29/025401/mmedia)). All computations were performed using MATLAB R2014a or newer (The MathWorks, Inc.).

A Laplacian prior was used in the regularisation with a hyperparameter value of 0.08. The hyperparameter was empirically chosen. In the simulation studies, the reconstructions were computed using meshes that were coarser than those used for simulating the data to avoid inverse crime. In all simulations and experimental reconstructions, we used the EIDORS complete electrode model with an electrode impedance of  $z = 0.01$ .

### 3. Results of the numerical analysis

The LAFR-rEIT electrode configurations (presented in section 2.3) were numerically analysed with the phantom with two inclusions. To show the performance of LAFR-rEIT as a function of number of rotational measurement positions, we present reconstructions using OPP4 configuration from single (no rotation) up to 256 rotational measurement positions in 180° rotation, presented in figure 6. As was expected, when the object was not rotated, the quality of the reconstruction was very poor: only the larger inclusion was seen and the reconstruction resolution was inadequate. However, when the number of rotational measurement positions was increased, the shape and location of the larger inclusion was improved. Moreover, when the number of measurement positions was increased to 32, the smaller inclusion was also detected by LAFR-rEIT. Increasing the number of positions from 32

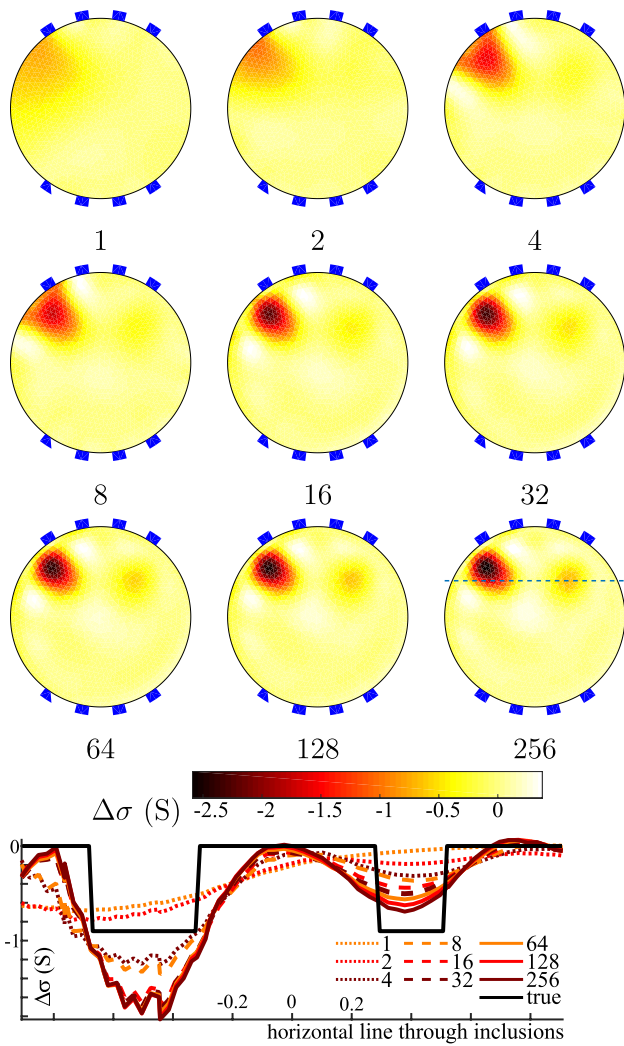


**Figure 6.** Development of reconstructions with respect to number of measurement positions 1–256 with electrode configuration OPP4. Conductivity profiles along a horizontal line through both inclusions are shown in the lower graph. The location of the horizontal lines is shown on top of the reconstruction with 256 measurement positions.

further improved the reconstruction. Although, this improvement was rather small after 64 positions, as seen in the reconstruction conductivity profiles along the inclusions in figure 6.

A 16-electrode configuration was analysed from 1 to 6 rotational measurement positions, as is shown in figure 7, for comparison to previous rEIT approaches. Small improvements in accuracy were also achieved in the 16-electrode model by increasing the amount of data through rotation.

The feasibility of additional LAFR-rEIT electrode configurations OPP2, OPP3, OPP4 + 2, HALF4, HALF6 and HALF8 are shown in figure 8. Symmetrical configurations OPP2 and OPP3 were reconstructed from simulated data with 32 rotational measurement positions in 180° rotation and asymmetrical OPP4 + 2, HALF4, HALF6 and HALF8 from data with 64 rotational measurement positions in 360° rotation. Thus, angular difference between rotational measurement positions

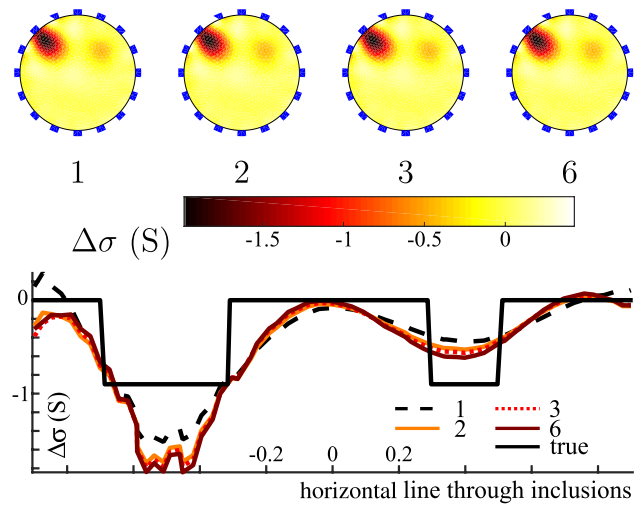


**Figure 7.** Reconstructions of the phantom using FULL16 electrode stepping model with 1, 2, 3, and 6 rotational measurement positions and respective conductivity profiles along a horizontal line passing through the centres of the inclusions, as shown in figure 6.

was the same in all cases. It is obvious from the reconstructions that accuracy was increased as the number of electrodes was increased. Configurations OPP4 + 2 and HALF8 found both inclusions, whereas in others the smaller is totally or almost invisible.

Visually, reconstructions with the 16-electrode model in figure 7 compared with the eight electrode LAFR-rEIT setups OPP4 (figure 6) and HALF8 (figure 8(f)) are very close to each other, when at least 32 (OPP4) or 64 (HALF8) rotational measurement positions were used. The plotted conductivity profiles through both inclusions in figure 9 support this observation, as the profiles differed only slightly in the conductivity of the larger inclusion and followed each other closely elsewhere.

#### 4. Results of the experimental analysis

We studied LAFR-rEIT experimentally using the OPP4 electrode configuration and three phantoms. The reconstructions were obtained using data from 1, 4, 16 and 32 rotational measurement positions in 180° rotation. The pictures and corresponding reconstructions in difference mode are shown in figure 10. In addition, the conductivity profiles along a line through the centres of the inclusions are shown for each case.

As was expected, and already seen in the simulated studies, a single measurement (without rotation) with OPP4 configuration did not provide enough information for good quality reconstruction. Then inclusions were only visible if they were close to the electrodes, as in case (3). By increasing the amount of data through rotation, most of the inclusions were detected by LAFR-rEIT already with 4 rotational measurement positions. Image accuracy and contrast were further improved as rotational measurement positions were increased, as can be seen visually and in the conductivity profiles.

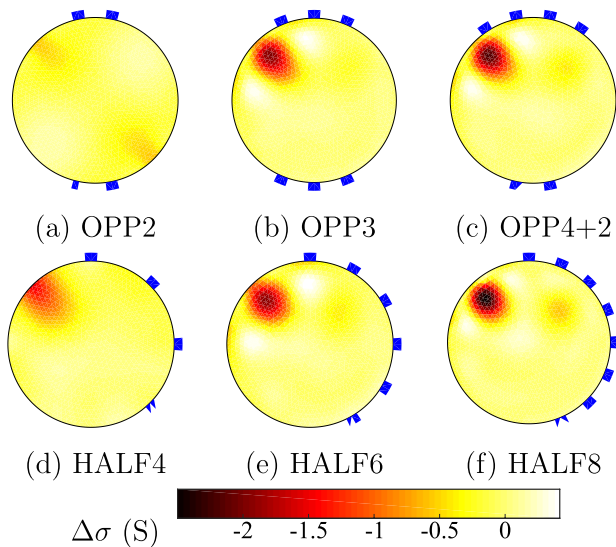


**Figure 8.** Reconstructions of additional LAFR-rEIT electrode configurations using (a), (b) 32 rotational measurement positions in  $180^\circ$  rotation and (c)–(f) 64 rotational measurement positions in  $360^\circ$  rotation.

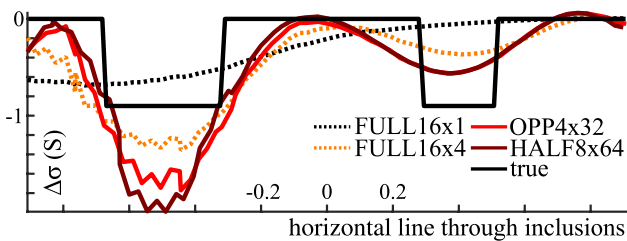


**Figure 9.** Comparison between 16- and 8-electrode models, the former with 1 and 6 rotational measurement positions (denoted FULL16  $\times$  1 and FULL16  $\times$  6) and the latter with the models OPP4 and HALF8 with 32 or 64 rotational measurement positions, respectively (denoted OPP4  $\times$  32 and HALF8  $\times$  64). The location of the horizontal lines is represented in figure 6.

## 5. Discussion

In this work, we have presented a new approach to rEIT where the angular span of the electrodes over the surface of the object is limited. The main motivation for the development of limited angle full revolution rotational EIT (LAFR-rEIT) was to enable multimodal imaging. Traditionally electrodes span over the object surface completely, and therefore the attachment of other measurement devices simultaneously is difficult. The simulated and experimental analysis results prove the potential of the approach in solving this problem.

In addition to demonstrating the LAFR-rEIT, we have developed functionality for the open source EIDORS package that solves the forward and inverse problems of EIT in the presented rotational setting. The developed functions are applicable to any feasible electrode configuration. In previous approaches on rEIT [4], additional electrodes have been added to model the rotation of the object. Another option is to rotate the nodes of the finite element mesh and change the nodes of the electrodes to correspond with the rotation. This approach has been noted to work well [7]. However, in the worst case when using several rotational measurement positions, amount

of boundary nodes explodes if each electrode requires separate nodes for each rotational coordinate. In this study, rotation was taken into account using a mapping matrix that describes rotation in a more realistic manner and models only the actual electrodes with controlled amount of boundary nodes. Also, rotation inside an already constructed finite element mesh preserves the electrode structure. Our EIDORS codes are provided in the supplementary material.

According to 2D numerical analysis, the eight electrode configurations OPP4 and HALF8 are the most promising ones in LAFR-rEIT. However, we note that the optimal setup depends on a variety of factors, including the geometry of the measured specimen. With the presented inversion model, using measurement data from 32 (OPP4) or 64 (HALF8) rotational measurement positions, reconstructions of conductivity change distributions are very similar compared to the reconstructions based on the 16-electrode rEIT with full surface coverage.

We found that rotational data from 32 to 64 measurement positions is a ‘sweet spot’ in terms of accuracy and computing time for eight electrode LAFR-rEIT using configurations OPP4 and HALF8. Reconstruction quality still benefits significantly from the additional data and computing time is in the order of minutes. LAFR-rEIT reconstruction from 128 and 256 rotational measurement positions was impossible to compute using a 8 Gb RAM computer. If memory is available, computing times are in the order of one to a few hours and the increase in accuracy achieved is relatively small. The issue with memory is due to full matrix operations in current implementation of the rotation. The eventual saturation of reconstruction quality is in accordance with previous 16-electrode rEIT studies [4, 7].

The feasibility of LAFR-rEIT was also verified with experimental measurements using OPP4 configuration. Resistive inclusions in the gelatine phantoms were detected using only 4 rotational measurement positions, but accuracy and contrast were significantly enhanced when measurement positions were increased up to 32 that was a feasible amount of rotations when done manually.

The amount of data acquired depends on the used stimulation and measurement pattern, the number of electrodes and the rotational measurement positions used. Using all tetrapolar combinations possible with eight electrodes and 64 measurement positions, results in  $64 \cdot 28 \cdot 15 = 26\,880$  independent measurements (28 different current injections and 15 measuring electrode pairs). Using all tetrapolar combinations possible with 16 electrodes and 6 measurement positions, results in  $6 \cdot 120 \cdot 91 = 65\,520$  independent measurements (120 injections and 91 measuring pairs). However, many of the tetrapolar measurements have low sensitivity. For example, in a conventional 16-electrode configuration, when current is injected between electrodes 1 and 2, most of the pairwise voltage measurements have low sensitivity. Hence, the amount of significant data is of the same order between 8-electrode LAFR-rEIT and 16-electrode rEIT, which justifies the comparable quality of the reconstructions in line with the lead field theory.



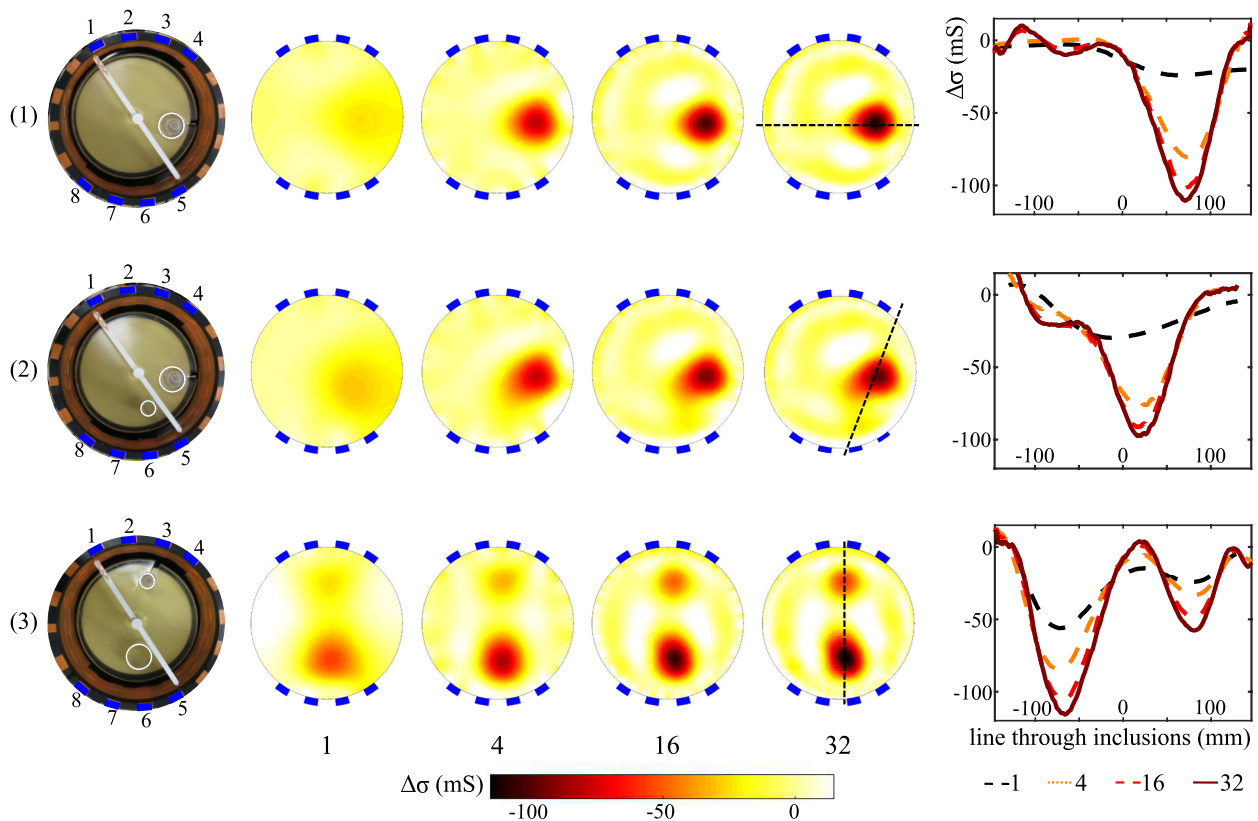


**Figure 10.** Experimental cases (1)–(3) and corresponding reconstructions using 1–32 rotational measurement positions in 180° rotation. Resistive inclusions are highlighted with white circles in the photographs. Conductivity profiles along a line passing through the centres of the inclusions are shown on the right. The locations of the lines are shown on top of the reconstructions with 32 measurement positions.

Rotational mapping  $M$  produces small local variations between neighbouring elements of the finite element mesh, as can be seen in figure 2. This is one limiting factor on the resolution of our method with a high number of rotational measurement positions. The advantage of the method is, however, the flexibility in accepting any configuration of electrodes and number of rotational measurement positions. By restricting these flexibilities, optimisation of the mapping may be possible for that specific application.

Other than numerical improvements, further interesting research includes whether other limited angle electrode configurations are feasible. This choice depends heavily on the needs of the multimodal instrumentation. Configurations can be studied in terms of the number and placement of the electrodes [23] as well as in terms of their size compared with the object size.

## 6. Conclusion

In this paper we introduced a novel approach to rEIT, where eight electrodes were distributed unevenly covering only half the surface of the object. In LAFR-rEIT, the object is rotated for 180° or 360°, depending on the electrode configuration, in aqueous solution, and several measurements are taken in different rotational positions to acquire information from all

parts the object. The conductivity change distribution is then reconstructed using novel finite element mesh modification that is available for EIDORS package.

We show here that LAFR-rEIT works using both simulated and experimental measurements and that LAFR-rEIT reconstructions are of the same quality as in previously published results of 16-electrode rEIT. The LAFR-rEIT approach offers new possibilities for multimodal imaging as it enables attaching other sensors simultaneously with EIT. The method is promising for biomedical imaging but also in other fields, such as non-destructive industrial process imaging.

## Acknowledgments

This work is funded by Jane and Aatos Erkkö Foundation, Instrumentarium Science Foundation, TEKES Human Spare Parts project and Academy of Finland (projects 270174 and 303801). The authors would like to thank Tuomo Savolainen and Panu Kuusela (University of Eastern Finland) for the help in the laboratory measurements.

## Conflicts of interest

The authors declare that they have no conflicts of interest.

## ORCID iDs

Mari Lehti-Polojärvi  <https://orcid.org/0000-0001-9826-5741>  
 Olli Koskela  <https://orcid.org/0000-0002-3424-9969>  
 Aku Seppänen  <https://orcid.org/0000-0002-4042-2254>  
 Edite Figueiras  <https://orcid.org/0000-0002-9824-3507>  
 Jari Hyttinen  <https://orcid.org/0000-0003-1850-3055>

## References

- [1] Webster J G 1990 *Electrical Impedance Tomography* (London: Taylor and Francis)
- [2] Holder D S 2004 *Electrical Impedance Tomography: Methods, History and Applications* (Boca Raton, FL: CRC Press)
- [3] Murphy S and York T 2006 Electrical impedance tomography with non-stationary electrodes *Meas. Sci. Technol.* **17** 3042
- [4] Huang C-N, Yu F-M and Chung H-Y 2007 Rotational electrical impedance tomography *Meas. Sci. Technol.* **18** 2958
- [5] Huang C-N, Yu F-M and Chung H-Y 2008 The scanning data collection strategy for enhancing the quality of electrical impedance tomography *IEEE Trans. Instrum. Meas.* **57** 1193–8
- [6] Zhang X, Chatwin C and Barber D 2015 A feasibility study of a rotary planar electrode array for electrical impedance mammography using a digital breast phantom *Physiol. Meas.* **36** 1311
- [7] Murphy E K, Mahara A and Halter R J 2017 Absolute reconstructions using rotational electrical impedance tomography for breast cancer imaging *IEEE Trans. Med. Imaging* **36** 892–903
- [8] Soleimani M 2006 Electrical impedance tomography imaging using *a priori* ultrasound data *Biomed. Eng. online* **5** 8
- [9] Grychtol B, Lionheart W, Wolf G, Bodenstern M and Adler A 2011 The importance of shape: thorax models for GREIT *Conf. EIT*
- [10] Borsic A, Syed H, Halter R and Hartov A 2011 Using ultrasound information in EIT reconstruction of the electrical properties of the prostate *Conf. EIT*
- [11] Crabb M G *et al* 2014 Mutual information as a measure of image quality for 3d dynamic lung imaging with EIT *Physiol. Meas.* **35** 863
- [12] Karhunen K, Seppänen A, Lehtikoinen A, Monteiro P J and Kaipio J P 2010 Electrical resistance tomography imaging of concrete *Cement Concr. Res.* **40** 137–45
- [13] Sun T, Tsuda S, Zauner K-P and Morgan H 2010 On-chip electrical impedance tomography for imaging biological cells *Biosens. Bioelectron.* **25** 1109–15
- [14] Somersalo E, Cheney M and Isaacson D 1992 Existence and uniqueness for electrode models for electric current computed tomography *SIAM J. Appl. Math.* **52** 1023–40
- [15] Vauhkonen M 1997 Electrical impedance tomography and prior information *PhD Thesis* University of Kuopio
- [16] Geselowitz D B 1971 An application of electrocardiographic lead theory to impedance plethysmography *IEEE Trans. Biomed. Eng.* **18** 38–41
- [17] Kauppinen P K, Hyttinen J A, Kööbi T and Malmivuo J 1999 Lead field theoretical approach in bioimpedance measurements: towards more controlled measurement sensitivity *Ann. New York Acad. Sci.* **873** 135–42
- [18] Kauppinen P, Hyttinen J and Malmivuo J 2006 Sensitivity distribution visualizations of impedance tomography measurement strategies *Int. J. Bioelectromagn.* **8** 1–9
- [19] Canali C, Mazzoni C, Larsen L B, Heiskanen A, Martinsen Ø G, Wolff A, Dufva M and Emnéus J 2015 An impedance method for spatial sensing of 3d cell constructs—towards applications in tissue engineering *Analyst* **140** 6079–88
- [20] Böttlich M, Tanskanen J M A and Hyttinen J A K 2017 Lead field theory provides a powerful tool for designing microelectrode array impedance measurements for biological cell detection and observation *Biomed. Eng. Online* **16** 85
- [21] Kourunen J 2014 Imaging of mixing in selected industrial processes using electrical resistance tomography *PhD Thesis* University of Eastern Finland ([http://publications.uef.fi/pub/urn\\_isbn\\_978-952-61-1638-9/urn\\_isbn\\_978-952-61-1638-9.pdf](http://publications.uef.fi/pub/urn_isbn_978-952-61-1638-9/urn_isbn_978-952-61-1638-9.pdf))
- [22] Adler A and Lionheart W R 2006 Uses and abuses of EIDORS: an extensible software base for EIT *Physiol. Meas.* **27** S25
- [23] Hyvonen N, Seppänen A and Staboulis S 2014 Optimizing electrode positions in electrical impedance tomography *SIAM J. Appl. Math.* **74** 1831–51